Large-Size Honeycomb-Shaped and Iris-Like Liquid Crystal Elastomer Actuators

Bin Ni, Gaoyu Liu, Mengxue Zhang, Patrick Keller, Michael Tatoulian, Min-Hui Li

CCS Chemistry

COMMUNICATION

Received: Jan. 21, 2021 | Accepted: Mar. 5, 2021

Large-Size Honeycomb-Shaped and Iris-Like Liquid Crystal Elastomer Actuators

Bin Ni[1], Gaoyu Liu[1], Mengxue Zhang[1], Patrick Keller[2]*, Michael Tatoulian[1]* & Min-Hui Li[1]*

[1]*Chimie ParisTech, Université Paris Sciences & Lettres, CNRS, Institut de Recherche de Chimie Paris, UMR8247, 75005 Paris,* [2]*Institut Curie, Université Paris Sciences & Lettres, CNRS, Sorbonne Université, Laboratoire Physico-Chimie Curie, UMR168, 75005 Paris*

**Corresponding authors: min-hui.li@chimieparistech.psl.eu; michael.tatoulian@chimieparistech.psl.eu; patrick.keller@curie.fr*

Cite this: *CCS Chem.* **2021**, *3*, 1081–1088

Nature is providing inspiration for researchers to mimic its functions or existing structures, which could remarkably promote the development of new materials. Here, a large-size honeycomb-shaped liquid crystal elastomer (LCE) actuator with LC orientation along the height of the honeycomb shape is built by combining magnetic field alignment and soft lithography technology. This homeotropic alignment allowed the height contraction of honeycomb and pore size expansion of hexagons in a reversible manner upon temperature variation. Therefore, this LCE actuator can be used as a structure for temperature-gated separation of particles. Another example is an iris-like LCE actuator, which has the capability of adjusting its aperture size with a temperature variation. Our approach provides a simple way to design customizable sophisticated LCE actuators for various potential applications.

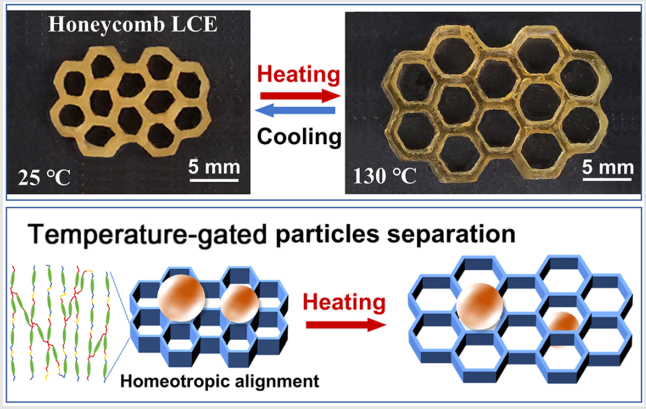

Keywords: **liquid crystal elastomers, soft actuators, biomimetic systems**

Introduction

Many biological systems exhibit either ingenious structures like the honeycomb or dynamic functionalities like the iris. New materials mimicking nature's sophisticated design are becoming an attractive research domain aimed to make a strong impact in technological advances. For example, smart polymers with the ability to sense multiple environmental variations and convert them into detectable active responses,[1–5] have attracted considerable interest. Liquid crystal elastomers (LCEs), initially discussed by De Gennes in 1975,[6] and later on by other investigators,[7–9] are one class of these smart materials. Oriented LCEs exhibit outstanding reversible anisotropic deformations upon various external stimuli such as temperature,[10] light,[11] pH change,[12] solvents,[13] and so forth. These excellent properties make them the polymeric materials of choice in various biomimetic applications such as biomimetic soft robots,[14–17] biomimetic self-cleaning surfaces,[18–20] iris regulation,[21,22] biomimetic flowers,[23] and so on.

Nevertheless, the complexity of biological systems brings many difficulties to the LCEs to further mimic their structures or motions, especially for some sophisticated

DOI: 10.31635/ccschem.021.202100818
CCS Chem. **2021**, *3*, 1081–1088

three-dimensional (3D) structures of large sizes. To obtain the reversible anisotropic deformations of LCEs, one of the prerequisites is the orientation of LC molecules in the sample. Taking nematic LCE as an example, the average macromolecular shape of nematic LC polymer is coupled with the nematic orientational order and is therefore elongated in the nematic phase. Upon nematic–isotropic (N–I) phase transition, a change of macromolecular shape is produced from elongated to spherical because the polymer chain recovers a random coil shape in the isotropic phase. In oriented LCE, where all mesogens are oriented uniformly in the whole sample (monodomain), the individual polymer chain shape change is translated to a macroscopic shape change of the elastomer at the N–I transition.[7] To make large-size LCEs with sophisticated 3D structures, the main challenge resides in the two somehow contradictory constraints, viz, making a molecularly oriented nematic liquid crystalline phase in a complex 3D volume. Frequently used approaches for the preparation of LCE actuators severely limit the possibilities of producing such sophisticated 3D structures. The mechanical stretch method proposed by Küpfer and Finkelmann[24] to obtain monodomain LCEs is suitable for large samples, but mainly in the form of films or fibers.[25] The popular surface alignment method[26–30] allows the preparation of LCE films with small and large areas but with a thickness of only ≤200 μm, intrinsically limited by the surface anchor force. The extrusion alignment method shows promising results, for example in 3D printing of LCEs; however, the orientation direction is restricted by the printer extrusion direction.[31]

Here, we revisited another alignment method, the magnetic field alignment, beneficial for aromatic LC molecules due to their exceptionally high diamagnetism. The aromatic rings tended to align their planes parallel to the magnetic field to minimize energy. A nematic polydomain sample without any treatment contains many tiny nematic monodomains with their optical axis (director *n*) oriented in many different directions, just as a crystal powder sample contains many crystallites. In the magnetic field, the tiny nematic monodomains of aromatic LC molecules could be oriented readily with their director *n* (typically, along the aromatic ring plane) parallel to the magnetic field because the magnetic coupling energy was larger than the thermal agitation energy (k_BT).[32] Consequently, a whole monodomain LC sample was obtained under magnetic field in the order of 0.1–1 T. As a 3D volume alignment method, magnetic alignment has been proved useful for fabricating oriented LCEs pillars of micrometer size[33,34] and films of centimeter size.[35,36] Also, there were a few reports on larger (up to 10 mm) sophisticated 3D LCEs by magnetic field alignment, especially iris-like tunable aperture[18] and large size of 3D freeforms with voxelated molecular patterning.[37] However, in these last examples, complex setups were used, for example, a multitude of pairs of magnets with a complicated configuration,[21] or a reorientable magnetic field (with magnets mounted on a rotation stage) combined with a digital micromirror device.[37] Herein, we proposed a simple and effective way to fabricate 3D LCE actuators with large sizes and sophisticated structures using a magnetic field combined with soft lithography.

For a long time, soft lithography has been used as the most popular method to replicate complex structures at different scales.[38] Keller's group[19,33,39] first prepared oriented LCE micropillars by combining magnetic field and soft lithography. In this work, we further developed a simple protocol to prepare large-size sophisticated 3D LCEs like honeycomb structure and iris-like structure with stimuli-responsive actuation properties (see Figure 1). Soft lithography was employed to customize these structures with sizes comparable with the actual sizes of the honeycomb (cell side ~3 mm) and human iris (inner and outer diameters ~4 and ~10 mm). A pair of magnets were chosen for the alignment of nematic monomers filled in the honeycomb-shaped or iris-like mold to get homeotropic orientation, that is, with the nematic director oriented along the hexagonal or cylindrical walls, and LCEs were finally obtained by photopolymerization. Notably, the homeotropic orientation was applied here to produce the desired actuation function. To the best of our knowledge, until now, little attention has been paid to homeotropic orientation in sophisticated 3D LCEs. At this point, it is necessary to recall an important property of LCEs: When a nematic LCE sample transits from the nematic to the isotropic phase, its volume remains constant for the following reasons.[40] First, because the volumetric thermal expansion coefficient of polymer materials is in the order of 10^{-4} (K^{-1}), the thermal expansion of LCEs is negligible. Second, the shear moduli of LCEs, like those of other classical elastomers, are only in the order of 10^{-4} times their compression moduli (a liquid-like behavior); therefore, LCEs essentially deform at constant volume during the thermally actuated contraction. This implies that the monodomain nematic LCE sample contracts in the direction of the nematic director but expands in the other two directions.[7,41] Consequently, taking advantage of this often-overlooked fundamental property, the fabricated large-size honeycomb-shaped LCE actuators can be used to separate selectively glass beads by size upon temperature change, and the iris-like LCE actuators can work as a temperature-controlled diaphragm. Moreover, beyond honeycomb-shaped and iris-like structures, this protocol provided a simple way to design other sophisticated LCE actuators for various potential applications.

Results and Discussion

The alignment and polymerization process to fabricate honeycomb-shaped LCEs is presented in Figure 1 (that for iris-like is similar). The honeycomb-shaped template

DOI: 10.31635/ccschem.021.202100818
CCS Chem. **2021**, *3*, 1081–1088

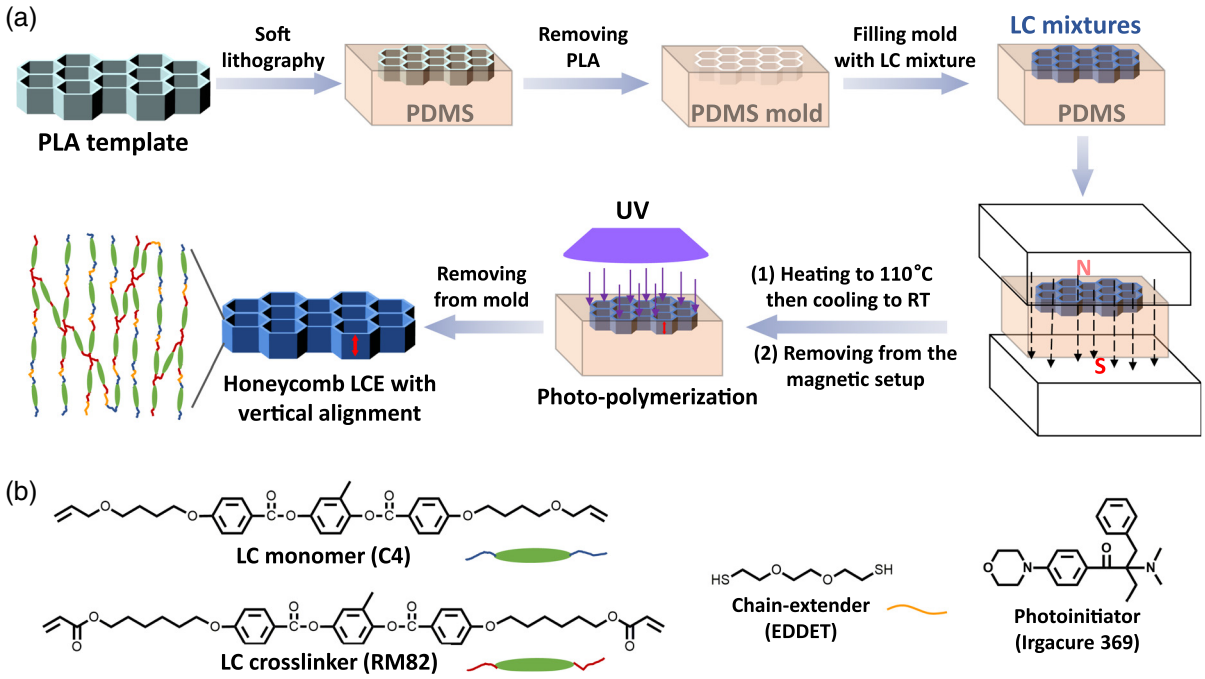

Figure 1 | *(a) The alignment and polymerization process to fabricate the honeycomb-shaped LCE actuator with homeotropic alignment where the schematic of the molecular organization is shown. (b) Chemical structures of the components in LC mixture.*

made of polylactic acid (PLA) was first produced by 3D printing. Then soft lithography method was employed to replicate a PLA template to a polydimethylsiloxane (PDMS) negative template called honeycomb mold. Each hexagon of the honeycomb template has the size of 2 mm (side) × 2 mm (height) × 0.5 mm (wall thickness) or 3 mm (side) × 3 mm (height) × 0.5 mm (wall thickness) (Supporting Information Figure S1). The thin hollow disk template had an outer diameter of 6 mm, an inner diameter of 3 mm, and 1 mm in thickness. The LC monomer mixture filled in the PDMS mold for LCEs preparation was comprised of the LC monomer 2-methyl-1,4-phenylene bis(4-(4-(allyloxy)butoxy)benzoate) (C4), the chain-extender (2,2′-(ethylenedioxy)diethanethiol) (EDDET), the LC cross-linker (2-methyl-1,4-phenylene bis(4-((6-(acryloyloxy)hexyl)oxy)benzoate)) (RM82), and the photoinitiator (2-benzyl-2-dimethylamino-1-(4-morpholinophenyl) butanone-1) (Irgacure 369) (Figure 1b). Their molar ratio was kept at C4:EDDET:RM82 = 1:1:0.4 in all experiments and the concentration of the photoinitiator Irgacure 369 was kept at 2 wt %. The prepared LC mixture maintained a nematic mesophase characteristic at room temperature for at least 4 days [see Supporting Information Figures S2a–S2c for differential scanning calorimetry (DSC) curves].[42] This provided the possibility to perform the photopolymerization conveniently at room temperature on the previously aligned nematic phase. Two permanent magnets with an adhesion strength of ~60 kg (~588 N) and remanence of 1.29–1.32 T were set facing and 3 cm-distancing from each other, which offered strong and homogeneous magnetic field to orientate the LC mixture (Figure 1 and Supporting Information Figure S3). The simulation of the magnetic flux density (*B*) by the finite element method using the commercial software COMSOL® (https://www.comsol.com/comsol-multiphysics) confirmed the good homogeneity of the magnetic field in the central area with the value of $B \sim 0.5$ T (see Supporting Information Figure S3b for simulation detail). The alignment of the LC mixture was achieved by first heating it to the isotropic phase (110 °C) and naturally cooling to room temperature (~0.5 °C/min). Finally, the aligned LC mixture was locked down in the "monodomain" nematic state by a thiol-ene/acrylate photopolymerization.[43–45] Figures 2a and 2b and Supporting Information Figures S4a and S4b show the final honeycomb-shaped LCEs with two fused hexagonal lattices and one hexagonal lattice peeled off the PDMS mold. The dimensions of the final honeycomb-shaped LCEs were slightly smaller than those of the initial mold [e.g., 1.8 mm (side) × 1.8 mm (height) × 0.5 mm (wall thickness) instead of 2 mm (side) × 2 mm (height) × 0.5 mm (wall thickness)] (Figures 2a and 2b). This might be due to polymerization stress during the photopolymerization process. The slightly irregular shape was caused by the pulling force when peeling LCE off the mold, and the structure became more regular upon heating with the stress relaxation, as shown in Figures 2b and 2d and Supporting Information Figure S4b.

DOI: 10.31635/ccschem.021.202100818
CCS Chem. **2021**, *3*, 1081–1088

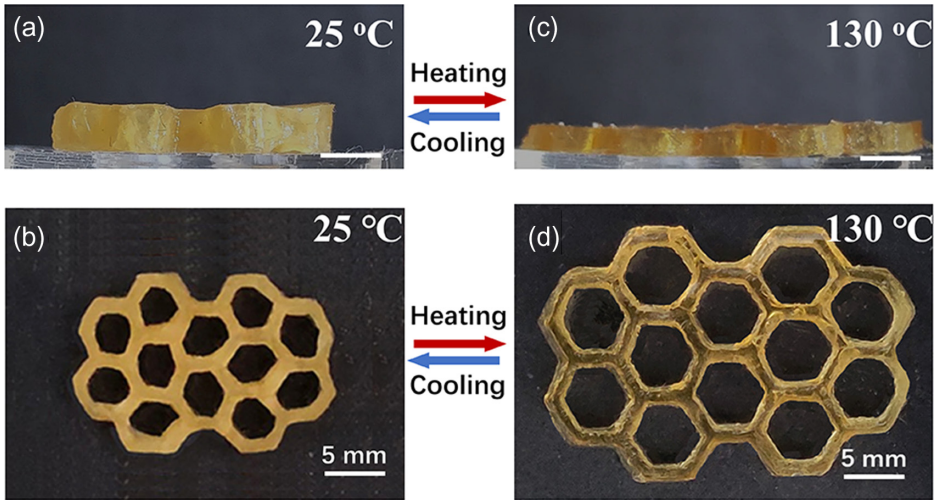

Figure 2 | *The honeycomb-shaped LCE actuator and its thermal deformation under thermal stimulation. (a and b) Side views. (c and d) Top views. The LCE contracts along with the height and expands in the other two directions reversibly upon heating and cooling. Scale bar = 5 mm.*

The alignment of LCE was also closely examined. A thin LCE film of ~160 μm thickness parallel to and beside the honeycomb wall in the same PDMS block (Figure 1a) was prepared. The LC mixtures before and after photopolymerization were first observed by polarizing optical microscopy (POM), as shown in Supporting Information Figure S5. The maximal birefringence was apparent in both the LC mixture and the thin LCE film when the nematic alignment direction was oriented at an angle of 45° relative to the polarizer. Finally, the LCE film was characterized by two-dimensional (2D) wide-angle X-ray scattering (WAXS), as shown in Figures 3a and 3b. The crescent-like signals along the *Y*-axis showed clearly that the nematic mesognes in LCE were oriented along this axis parallel to the magnetic field *B*. From these crescents, the nematic order parameter (*S*) was estimated to be $S \sim 0.5$ (according to an approach described previously[46]), and the average lateral distance between the mesogens was estimated to be 0.44 nm. The inner signals along the *X*-axis gave a distance of 2.3 nm, corresponding to the mesogen length. Thus, we inferred that the process used here allowed us to prepare effectively the aligned honeycomb-shaped LCE sample with a homeotropic orientation.

The honeycomb-shaped LCE frame was then heated to 130 °C (above the N–I phase transition of LCE, $T_{N-I} \sim 125$ °C; Supporting Information Figure S2d). A contraction in the height direction and expansions in the other two directions was observed (Figure 2c and 2d and Supporting Information Figure S4b and Video S1), in agreement with the fact that, essentially, the LCEs deformed at constant volume. Taking the two fused

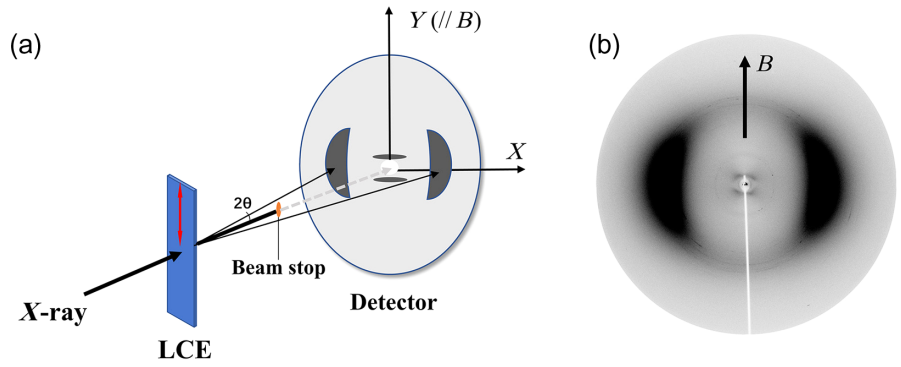

Figure 3 | *(a) The schematic illustration of the 2D WAXD experiment. (b) 2D WAXD pattern of LCE film. The red arrow indicates the orientation of the nematic director. The crescent-like signals along* Y*-axis (parallel to the magnetic field* B*) allow measuring the nematic order parameter as* S *~ 0.5 and the average lateral distance between mesogens as 0.44 nm. The inner signals along the* X*-axis give a distance of 2.3 nm corresponding to the mesogen length.*

DOI: 10.31635/ccschem.021.202100818
CCS Chem. **2021**, *3*, 1081–1088

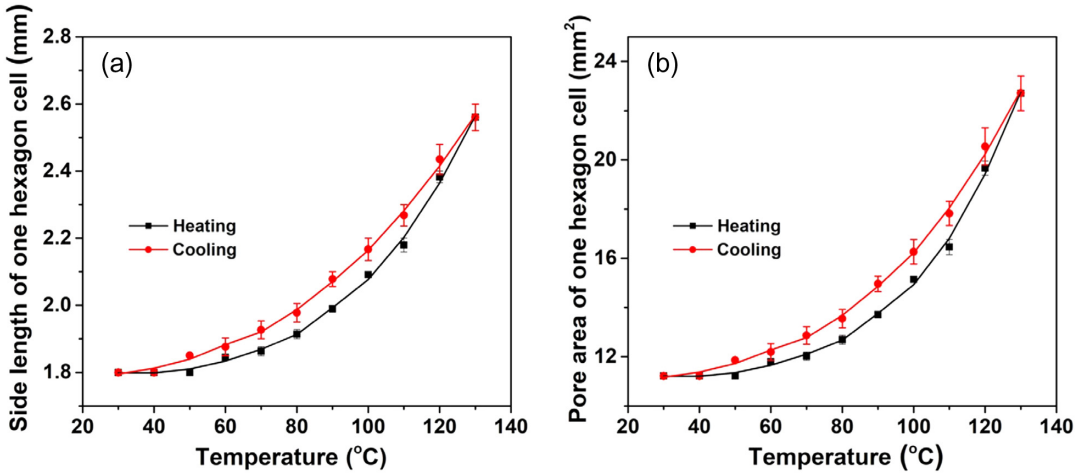

Figure 4 | *The dimensions of the honeycomb LCE actuator in Figure 2 as a function of temperature. (a) Side length variation of one hexagon cell. (b) Pore area variation of one hexagon cell.*

hexagonal lattices as an example, the side length of the hexagon ultimately changed from 1.8 to ~2.55 mm (Figure 4a), and the corresponding pore area of the hexagonal structure increased from 11 to 21 mm^2 (Figure 4b). Upon cooling down to room temperature, the honeycomb structure regained its original size (Supporting Information Video S1). Supporting Information Figure S6 provides a schematic of this size variation, resulting from changes in the mesogen order and polymer chain conformation in one wall of honeycomb LCE actuator at the N–I phase transition. The size variation of one-hexagonal-lattice honeycomb LCE upon heating and cooling is shown in Supporting Information Figure S7.

Such a significant change of the honeycomb structure suggested a potential application for temperature-gated passage and separation of particles. Figures 5a–5c and Supporting Information Video S2 show the temperature-gated passage of a 7 mm diameter ball from the central hole when the one-hexagonal-lattice honeycomb structure is heated up to 130 °C. To investigate the

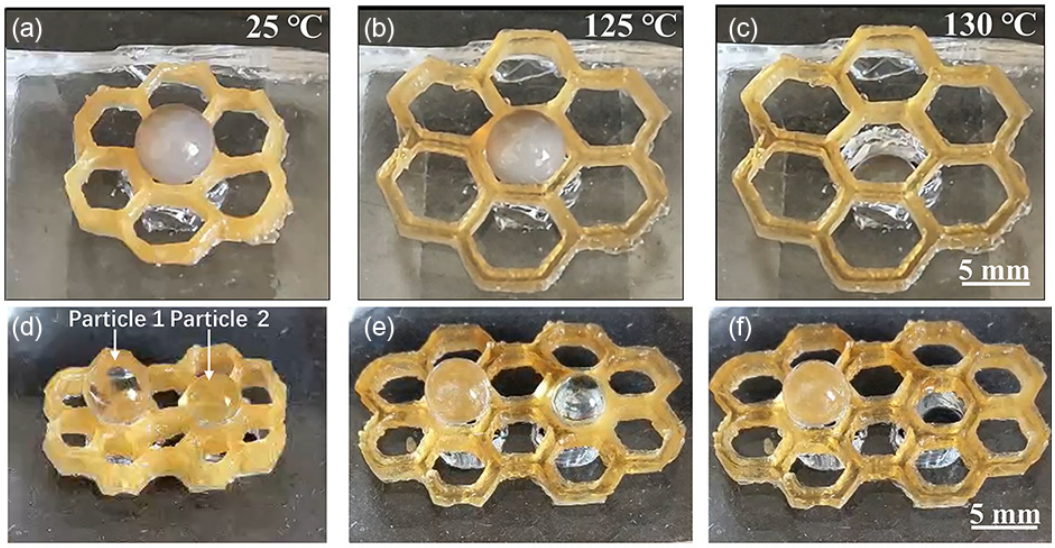

Figure 5 | *Honeycomb-shaped LCEs exhibit temperature-gated particle passage (a–c) and particles' separation (d–f). (a and d) 25 °C, (b and e) 125 °C, and (c and f) 130 °C. In (a–c), the ball diameter is 7 mm, and the initial side length of one hexagon is around 2.5 mm. In (e–f), the diameters of particles 1 and 2 are 5.2 and 4.2 mm, respectively; the initial side length of one hexagon is around 1.8 mm. The small color variation of the glass balls in (d–f) upon heating was caused by the reflection variation of the LCE color through transparent glass balls. The honeycomb frame was supported by a PDMS structure (for its transparency) and submerged in low viscosity silicone oil to reduce the friction between the LCE actuator and the glass beads.*

DOI: 10.31635/ccschem.021.202100818
CCS Chem. **2021**, *3*, 1081–1088

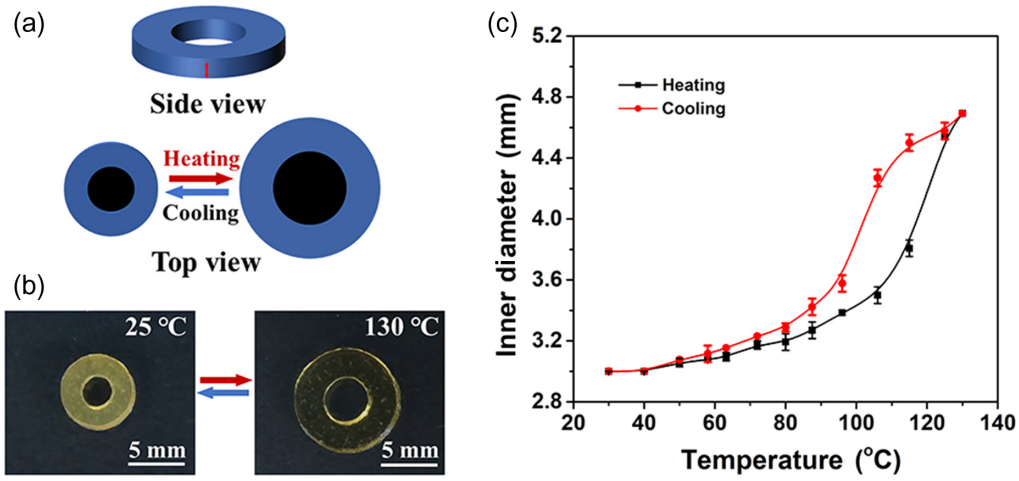

Figure 6 | *(a) Schematic illustration of iris-like LCE with homeotropic alignment (nematic director perpendicular to the disc surface). (b) The aperture of iris-like LCE changes reversibly between room temperature and 130 °C. (c) The aperture (inner-diameter) of iris-like LCE as a function of the temperature. The adjustable aperture size is actuated by thermal stimulation, demonstrating the controllability of iris contraction states.*

particle separation ability of this special structure, two glass balls with different diameters, D = 5.2 and 4.2 mm, were positioned on the two-hexagonal-lattice honeycomb frame. Due to the larger diameter of both balls than the pore size at room temperature, the balls could stand on the frame (Figure 5d). The pore size started to expand with temperature increase, which led to a glass ball with D = 4.2 mm sinking through the honeycomb structure (Figure 5e). Ultimately, this glass ball passed through the honeycomb pore successfully when the temperature reached 130 °C. Meanwhile, the glass ball with D = 5.2 mm remained on the top of the frame (Figure 5f and Supporting Information Video S3). In addition, multiple particle separation was also achieved with the same frame. Three glass beads with D = 5.2, 4.2, and 3.9 mm, respectively, were positioned on the honeycomb frame, and the two smaller beads were able to pass through the honeycomb structure one-by-one successively with temperature increase (Supporting Information Figure S8 and Video S4). Thus, by changing the temperature, the LCE honeycomb structure had the capacity of adjusting its pore diameter to separate particles by size. The results presented here could be extended readily to smaller or larger honeycomb structures and other particles with varying sizes and/or shapes.

Finally, by changing the characteristic shape of the PDMS mold, a homeotropically aligned thin hollow disk LCE actuator with an outer diameter of 6 mm, inner diameter of 3 mm, and a thickness of 1 mm was also designed (Figure 6). This actuator mimicked the dynamic function of the human iris with a tunable aperture. As shown in Figures 6a and 6b, the aperture size (inner diameter) of the LCE changed from 3 to 4.7 mm reversibly upon the heating–cooling stimulation cycle (Figures 6b and 6c, and Supporting Information Videos S5 and S6). Figure 6c demonstrates that the aperture of this iris-like LCE actuator could be modified continuously by temperature variation.

Conclusion

Inspired by natural structures, honeycomb-shaped and iris-like LCEs with real honeycomb and iris size scales were built via a combination of magnetic field alignment and soft lithography technology. These structures exhibited reversible deformation behaviors when thermally stimulated. The honeycomb LCE had a capacity of temperature-gated separation of particles by size. Thin iris-like hollow disk LCE showed tunable aperture controlled by temperature variations. The approach described in the present work provides a simple way to prepare complex, large-size 3D LCEs with sophisticated deformations, which might greatly benefit the manufacture of LCE soft robots and expand their future applications. Moreover, to better control the temperature variations necessary to drive the LCE actuators described currently, photothermally active dopants such as gold nanoparticles or carefully designed dyes could be introduced easily.[23,47] This work is in progress and might help to explore further the possible applications of LCE actuators with various sophisticated, or even exotic shapes and deformations prepared by this simple method.

Supporting Information

Supporting Information is available and includes experimental procedures and characterization data (PDF), actuation of honeycomb-shaped and iris-like LCE

DOI: 10.31635/ccschem.021.202100818
CCS Chem. **2021**, *3*, 1081–1088

(Videos S1, S5, and S6), and particle separation of honeycomb-shaped LCE (Videos S2, S3, and S4).

Conflict of Interest

There are no conflicts to declare.

Funding Information

This study received support from the French National Research Agency (ANR-16-CE29-0028) and from the "Institut Pierre-Gilles de Gennes" (IPGG, laboratoire d'excellence, "Investissements d'avenir" programs ANR-10-IDEX-0001-02 PSL, ANR10-LABX-31 and ANR-10-EQPX-34).

Acknowledgments

B.N. and G.L. gratefully acknowledge the China Scholarship Council for funding their Ph.D. scholarships. The authors would like to thank Rémy Fert and Eric Nicolau (the mechanical workshop of UMR168 CNRS in Institut Curie) for building the home-designed holder equipped with two permanent magnets, Chuanyu Zhang (Université de Paris) for the simulation of the magnetic field in this home-made setup, Bruno Pelat (Chimie ParisTech) for his help in the preparation of PLA templates by 3D printing, and Pierre-Antoine ALBOUY (Université Paris-Saclay) for the X-ray scattering experiments.

References

1. Mirfakhrai, T.; Madden, J. D. W.; Baughman, R. H. Polymer Artificial Muscles. *Mater. Today* **2007**, *10*, 30–38.
2. Son, D.; Kang, J.; Vardoulis, O.; Kim, Y.; Matsuhisa, N.; Oh, J. Y.; To, J. W. F.; Mun, J.; Katsumata, T.; Liu, Y.; McGuire, A. F.; Krason, M.; Molina-Lopez, F.; Ham, J.; Kraft, U.; Lee, Y.; Yun, Y.; Tok, J. B. H.; Bao, Z. An Integrated Self-Healable Electronic Skin System Fabricated via Dynamic Reconstruction of a Nanostructured Conducting Network. *Nat. Nanotech.* **2018**, *13*, 1057–1065.
3. White, T. J.; Broer, D. J. Programmable and Adaptive Mechanics with Liquid Crystal Polymer Networks and Elastomers. *Nat. Mater.* **2015**, *14*, 1087–1098.
4. Chen, Q.; Yu, X.; Pei, Z.; Yang, Y.; Wei, Y.; Ji, Y. Multi-Stimuli Responsive and Multi-Functional Oligoaniline-Modified Vitrimers. *Chem. Sci.* **2017**, *8*, 724–733.
5. Gelebart, A. H.; Jan Mulder, D.; Varga, M.; Konya, A.; Vantomme, G.; Meijer, E. W.; Selinger, R. L. B.; Broer, D. J. Making Waves in a Photoactive Polymer Film. *Nature* **2017**, *546*, 632–636.
6. De Gennes, P.-G. Physique Moleculaire—Reflexions sur un Type de Polymeres Nematiques. *CR Acad. Sci. Paris Ser. B* **1975**, *281*, 101–103.
7. Li, M. H.; Keller, P. Artificial Muscles Based on Liquid Crystal Elastomers. *Philos. Trans. A Math. Phys. Eng. Sci.* **2006**, *364*, 2763–2777.
8. Ohm, C.; Brehmer, M.; Zentel, R. Liquid Crystalline Elastomers as Actuators and Sensors. *Adv. Mater.* **2010**, *22*, 3366–3387.
9. Wani, O. M.; Verpaalen, R.; Zeng, H.; Priimagi, A.; Schenning, A. An Artificial Nocturnal Flower via Humidity-Gated Photoactuation in Liquid Crystal Networks. *Adv. Mater.* **2019**, *31*, 1805985.
10. Lu, H. F.; Wang, M.; Chen, X. M.; Lin, B. P.; Yang, H. Interpenetrating Liquid-Crystal Polyurethane/Polyacrylate Elastomer with Ultrastrong Mechanical Property. *J. Am. Chem. Soc.* **2019**, *141*, 14364–14369.
11. Pang, X.; Lv, J. A.; Zhu, C.; Qin, L.; Yu, Y. Photodeformable Azobenzene-Containing Liquid Crystal Polymers and Soft Actuators. *Adv. Mater.* **2019**, *31*, 1904224.
12. Shishmanova, I. K.; Bastiaansen, C. W.; Schenning, A. P.; Broer, D. J. Two-Dimensional pH-Responsive Printable Smectic Hydrogels. *Chem. Commun.* **2012**, *48*, 4555–4557.
13. Chang, C.-K.; Bastiaansen, C. M. W.; Broer, D. J.; Kuo, H.-L. Alcohol-Responsive, Hydrogen-Bonded, Cholesteric Liquid-Crystal Networks. *Adv. Func. Mater.* **2012**, *22*, 2855–2859.
14. Wani, O. M.; Zeng, H.; Priimagi, A. A Light-Driven Artificial Flytrap. *Nat. Commun.* **2017**, *8*, 15546.
15. Jiang, Z. C.; Xiao, Y. Y.; Tong, X.; Zhao, Y. Selective Decrosslinking in Liquid Crystal Polymer Actuators for Optical Reconfiguration of Origami and Light-Fueled Locomotion. *Angew. Chem. Int. Ed.* **2019**, *58*, 5332–5337.
16. Ahn, C.; Liang, X.; Cai, S. Bioinspired Design of Light-Powered Crawling, Squeezing, and Jumping Untethered Soft Robot. *Adv. Mater. Technol.* **2019**, *4*, 1900185.
17. Palagi, S.; Singh, D. P.; Fischer, P. Light-Controlled Micromotors and Soft Microrobots. *Adv. Opt. Mater.* **2019**, *7*, 1900370.
18. Li, C.; Zhang, Y.; Ju, J.; Cheng, F.; Liu, M.; Jiang, L.; Yu, Y. In Situ Fully Light-Driven Switching of Superhydrophobic Adhesion. *Adv. Funct. Mater.* **2012**, *22*, 760–763.
19. Wu, Z. L.; Buguin, A.; Yang, H.; Taulemesse, J.-M.; Le Moigne, N.; Bergeret, A.; Wang, X.; Keller, P. Microstructured Nematic Liquid Crystalline Elastomer Surfaces with Switchable Wetting Properties. *Adv. Func. Mater.* **2013**, *23*, 3070–3076.
20. Shahsavan, H.; Salili, S. M.; Jakli, A.; Zhao, B. Smart Muscle-Driven Self-Cleaning of Biomimetic Microstructures from Liquid Crystal Elastomers. *Adv. Mater.* **2015**, *27*, 6828–6833.
21. Schuhladen, S.; Preller, F.; Rix, R.; Petsch, S.; Zentel, R.; Zappe, H. Iris-like Tunable Aperture Employing Liquid-Crystal Elastomers. *Adv. Mater.* **2014**, *26*, 7247–7251.
22. Zeng, H.; Wani, O. M.; Wasylczyk, P.; Kaczmarek, R.; Priimagi, A. Self-Regulating Iris Based on Light-Actuated Liquid Crystal Elastomer. *Adv. Mater.* **2017**, *29*, 1701814.
23. Zuo, B.; Wang, M.; Lin, B.-P.; Yang, H. Photomodulated Tricolor-Changing Artificial Flowers. *Chem. Mater.* **2018**, *30*, 8079–8088.
24. Küpfer, J.; Finkelmann, H. Nematic Liquid Single Crystal Elastomers. *Makromol. Chem. Rapid Comm.* **1991**, *12*, 717–726.

DOI: 10.31635/ccschem.021.202100818
CCS Chem. **2021**, *3*, 1081–1088

25. Ula, S. W.; Traugutt, N. A.; Volpe, R. H.; Patel, R. R.; Yu, K.; Yakacki, C. M. Liquid Crystal Elastomers: An Introduction and Review of Emerging Technologies. *Liq. Cryst. Rev.* **2018**, *6*, 78–107.
26. Xia, Y.; Zhang, X.; Yang, S. Instant Locking of Molecular Ordering in Liquid Crystal Elastomers by Oxygen-Mediated Thiol-Acrylate Click Reactions. *Angew. Chem. Int. Ed.* **2018**, *57*, 5665–5668.
27. de Haan, L. T.; Sanchez-Somolinos, C.; Bastiaansen, C. M.; Schenning, A. P.; Broer, D. J. Engineering of Complex Order and the Macroscopic Deformation of Liquid Crystal Polymer Networks. *Angew. Chem. Int. Ed.* **2012**, *51*, 12469–12472.
28. Li, M. H.; Keller, P.; Li, B.; Wang, X.; Brunet, M. Light-Driven Side-On Nematic Elastomer Actuators. *Adv. Mater.* **2003**, *15*, 569–572.
29. Ma, S.; Li, X.; Huang, S.; Hu, J.; Yu, H. A Light-Activated Polymer Composite Enables On-Demand Photocontrolled Motion: Transportation at the Liquid/Air Interface. *Angew. Chem. Int. Ed.* **2019**, *58*, 2655–2659.
30. Li, X.; Ma, S.; Hu, J.; Ni, Y.; Lin, Z.; Yu, H. Photo-Activated Bimorph Composites of Kapton and Liquid-Crystalline Polymer towards Biomimetic Circadian Rhythms of Albizia Julibrissin Leaves. *J. Mater. Chem. C* **2019**, *7*, 622–629.
31. Ambulo, C. P.; Burroughs, J. J.; Boothby, J. M.; Kim, H.; Shankar, M. R.; Ware, T. H. Four-Dimensional Printing of Liquid Crystal Elastomers. *ACS Appl. Mater. Interfaces* **2017**, *9*, 37332–37339.
32. De Gennes, P. G.; Prost, J. *The Physics of Liquid Crystal*; Clarendon Press: Oxford, UK, **1993**.
33. Buguin, A.; Li, M. H.; Silberzan, P.; Ladoux, B.; Keller, P. Micro-Actuators: When Artificial Muscles Made of Nematic Liquid Crystal Elastomers Meet Soft Lithography. *J. Am. Chem. Soc.* **2006**, *128*, 1088–1089.
34. Yao, Y.; Waters, J. T.; Shneidman, A. V.; Cui, J.; Wang, X.; Mandsberg, N. K.; Li, S.; Balazs, A. C.; Aizenberg, J. Multi-responsive Polymeric Microstructures with Encoded Predetermined and Self-Regulated Deformability. *Proc. Natl. Acad. Sci. U. S. A.* **2018**, *115*, 12950–12955.
35. Li, M. H.; Keller, P.; Yang, J.; Albouy, P. A. An Artificial Muscle with Lamellar Structure Based on a Nematic Triblock Copolymer. *Adv. Mater.* **2004**, *16*, 1922–1925.
36. Petsch, S.; Rix, R.; Khatri, B.; Schuhladen, S.; Müller, P.; Zentel, R.; Zappe, H. Smart Artificial Muscle Actuators: Liquid Crystal Elastomers with Integrated Temperature Feedback. *Sens. Actuat. A Phys.* **2015**, *231*, 44–51.
37. Tabrizi, M.; Ware, T. H.; Shankar, M. R. Voxelated Molecular Patterning in Three-Dimensional Freeforms. *ACS Appl. Mater. Interfaces* **2019**, *11*, 28236–28245.
38. Duffy, D. C.; McDonald, J. C.; Schueller, O. J. A.; Whitesides, G. M. Rapid Prototyping of Microfluidic Systems in Poly(dimethylsiloxane). *Anal. Chem.* **1998**, *70*, 4974–4984.
39. Yang, H.; Buguin, A.; Taulemesse, J. M.; Kaneko, K.; Mery, S.; Bergeret, A.; Keller, P. Micron-Sized Main-Chain Liquid Crystalline Elastomer Actuators with Ultralarge Amplitude Contractions. *J. Am. Chem. Soc.* **2009**, *131*, 15000–15004.
40. Warner, T.; Terentjev, E. M. *Liquid Crystal Elastomers*; Oxford University Press: UK, **2003**.
41. An, N.; Li, M.; Zhou, J. Instability of Liquid Crystal Elastomers. *Smart Mater. Struct.* **2015**, *25*, 015016.
42. Ni, B.; Zhang, M.; Guyon, C.; Keller, P.; Tatoulian, M.; Li, M. H. Plasma-Induced Polymerizations: A New Synthetic Entry in Liquid Crystal Elastomer Actuators. *Macromol. Rapid Commun.* **2020**, *41*, 2000385.
43. Ware, T. H.; Perry, Z. P.; Middleton, C. M.; Iacono, S. T.; White, T. J. Programmable Liquid Crystal Elastomers Prepared by Thiol–Ene Photopolymerization. *ACS Macro Lett.* **2015**, *4*, 942–946.
44. Hessberger, T.; Braun, L.; Zentel, R. Microfluidic Synthesis of Actuating Microparticles from a Thiol-Ene Based Main-Chain Liquid Crystalline Elastomer. *Polymers* **2016**, *8*, 410.
45. De Bellis, I.; Ni, B.; Martella, D.; Parmeggiani, C.; Keller, P.; Wiersma, D. S.; Li, M.-H.; Nocentini, S. Color Modulation in Morpho Butterfly Wings Using Liquid Crystalline Elastomers. *Adv. Intell. Syst.* **2020**, *2*, 2000035.
46. Davidson, P.; Petermann, D.; Levelut, A. M. The Measurement of the Nematic Order Parameter by X-ray Scattering Reconsidered. *J. Phys. II* **1995**, *5*, 113–131.
47. Liu, X.; Wang, X.; Liu, T.; Keller, P. Gold Nanoparticles Incorporated Nematic Gel Micropillars Capable of Laser Actuation at Room Temperature. *Macromolecules* **2016**, *49*, 8322–8331.

DOI: 10.31635/ccschem.021.202100818
CCS Chem. **2021**, *3*, 1081–1088